Properties of The Discrete Sinc Quantum State and Applications to Measurement Interpolation

Charlee Stefanski[1,2], Vanio Markov[1], and Constantin Gonciulea[1]

[1]Wells Fargo

[2]UC Berkeley

arXiv:2207.00564v1 [quant-ph] 1 Jul 2022

Extracting the outcome of a quantum computation is a difficult task. In many cases, the quantum phase estimation algorithm is used to digitally encode a value in a quantum register whose amplitudes' magnitudes reflect the discrete sinc function. In the standard implementation the value is approximated by the most frequent outcome, however, using the frequencies of other outcomes allows for increased precision without using additional qubits. One existing approach is to use Maximum Likelihood Estimation, which uses the frequencies of all measurement outcomes. We provide and analyze several alternative estimators, the best of which rely on only the two most frequent measurement outcomes. The Ratio-Based Estimator uses a closed form expression for the decimal part of the encoded value using the ratio of the two most frequent outcomes. The Coin Approximation Estimator relies on the fact that the decimal part of the encoded value is very well approximated by the parameter of the Bernoulli process represented by the magnitudes of the largest two amplitudes. We also provide additional properties of the discrete sinc state that could be used to design other estimators.

1 Introduction

Quantum phase estimation is a fundamental method in quantum computing, used as a building block in many other quantum algorithms, such as Shor's and quantum amplitude estimation. Its core underlying procedure first creates an analog representation of a periodic signal into quantum state, and then digitally encodes the period of this signal into the state of a quantum register that can be efficiently measured.

We refer to this quantum state with remarkable properties as "discrete sinc", the "period encoding state", the "phase estimation state", or the "interpolation state", because after a phase correction, its amplitudes match the interpolation coefficients in the classical interpolation theorem [1, 2]. We call the resulting outcome probability distribution the "discrete sinc squared" distribution or "the Fejér distribution" because its probabilities match the coefficients in Fejér kernels [3, 4]. We used this state and the underlying procedure in the quantum phase estimation algorithm to encode discrete functions, or dictionaries, into quantum state, and interpolate non-integer values [2].

While the canonical phase/amplitude estimation algorithms use digital encoding of a value to estimate it, efforts have been made to improve the accuracy of those estimates by interpolating "in-between" the discrete values. In particular, Maximum Likelihood Estimation has been used to post-process measurement results and improve the estimation precision without additional qubits [5].

In this paper we present additional properties of the discrete sinc quantum state and Fejér distribution and provide alternative estimation methods. We provide closed-form estimators for the expressions for the encoded value, that use consecutive pairs of amplitudes as inputs. The pair with the highest magnitudes is the most useful, and we show that it can be used to represent a

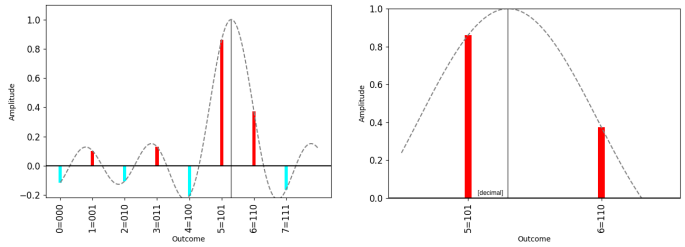


Figure 1: Left: Histogram of the amplitudes of a 3-qubit quantum state with the encoded value 5.3 compared to the discrete sinc function. Right: The two largest amplitudes of the state, which can be used to estimate the decimal part of the encoded value.

Bernoulli process, i.e. a (biased) coin, whose parameter (bias) is an estimate for the decimal part of the encoded value. We also show that the equation that needs to be solved in order to find the Maximum Likelihood Estimate is a form of interpolation in the context of the Fejér distribution.

2 Preliminaries

The sinc function is common in digital signal processing [6]. It can be defined on a set of real numbers as

$$\begin{aligned}\operatorname{sinc}(t) &= \begin{cases} 1, & \text{if } t = 0 \\ \frac{\sin(t)}{t}, & \text{otherwise} \end{cases} \\ &= \prod_{j=1}^{\infty} \cos\left(\frac{t}{2^j}\right)\end{aligned}$$

For a positive integer n and a real number t the function sincd_n is defined as

$$\operatorname{sincd}_n(t) = \frac{\operatorname{sinc}(t)}{\operatorname{sinc}\left(\frac{t}{2^n}\right)} = \prod_{j=1}^{n} \cos\left(\frac{t}{2^j}\right).$$

For a real number t, the normalized versions of the sinc and sincd functions are defined as $\operatorname{sinc}_\pi(t) = \operatorname{sinc}(\pi t)$ and $\operatorname{sincd}_{\pi,n}(t) = \operatorname{sincd}_n(\pi t)$, respectively.

Given a positive integer n and a real number $t \in [0, N)$, where $N = 2^n$, consider the quantum state

$$|\phi_{n,t}\rangle = \sum_{k=0}^{N-1} e^{i\pi \frac{N-1}{N}(t-k)} c_{N,t}(k) \, |k\rangle_n \tag{1}$$

where

$$\begin{aligned} c_{N,t}(k) &= \begin{cases} 1, & \text{if } t = k \\ \frac{1}{N} \frac{\sin((t-k)\pi)}{\sin((t-k)\frac{\pi}{N})}, & \text{otherwise} \end{cases} \\ &= \operatorname{sincd}_{\pi,n}(t-k) \\ &= \prod_{j=1}^{n} \cos\left((t-k)\frac{\pi}{2^j}\right). \end{aligned}$$

Note that the amplitudes in the state add up to 1:

$$\sum_{k=0}^{N-1} e^{i\pi \frac{N-1}{N}(t-k)} c_{N,t}(k) = 1. \tag{2}$$

This state encodes the result of the phase estimation algorithm, also used in the amplitude estimation algorithm, and to encode values and functions [2, 7].

If $t \in [0, N)$ is not an integer, the probability mass function of the measurement distribution for the $|\phi_{n,t}\rangle$ quantum state is

$$p_{N,t}(k) = \frac{1}{N^2} \frac{\sin^2((t-k)\pi)}{\sin^2((t-k)\frac{\pi}{N})} \tag{3}$$

for $0 \leq k < N$.

The values of $p_{N,t}$ match those of the normalized Fejér kernel [3, 4].

Lemma 2.1 (MLE Property)**.** *With the notations above, the following identity holds for a non-integer $t \in [0, N)$:*

$$\frac{1}{N} \sum_{k=0}^{N-1} p_{N,t}(k) \cot((t-k)\frac{\pi}{N}) = \cot(t\pi) \tag{4}$$

This property allows for the estimation of the non-integer parameter $t \in [0, N)$ of a given quantum state $|\phi_{n,t}\rangle$ by repeated measurement [5]. The estimation as a real number is more precise than the one obtained by just using the integer outcomes of a measurement, as in the standard phase estimation algorithm.

Equivalent forms of this equation are:

$$\frac{1}{N} \sum_{k=0}^{N-1} (1 - p_{N,t}(k)) \cot((t-k)\frac{\pi}{N}) = 0,$$

and

$$\sum_{k=0}^{N-1} p_{N,t}(k)(-1)^k \cos((t-k)\frac{\pi}{N}) c_{N,t}(k) = \cos(t\pi).$$

Estimating the parameter t of the period encoding state $|\phi_{n,t}\rangle$ and its corresponding probability distribution $p_{N,t}$ from the function q is a statistical inference task. We are looking for the estimate $\hat{t} \in [0, N)$ such that the distribution $p_{N,\hat{t}}$ is the best fit for the function q obtained through measurement.

Kullback–Leibler divergence or maximum likelihood estimation. The relative entropy, or the Kullback–Leibler divergence, from q to $p_{N,t}$ is

$$\begin{aligned} D_{KL}(q \parallel p_{N,t}) &= \sum_{k=0}^{N-1} q(k) \log\left(\frac{q(k)}{p_{N,t}(k)}\right) \\ &= \sum_{k=0}^{N-1} q(k) \log(q(k)) - \log \mathcal{L}(t|q) \end{aligned}$$

where

$$\mathcal{L}(t|q) = \prod_{k=0}^{N-1} p_{N,t}(k)^{q(k)}$$

is the likelihood of the parameter t given the measurement reflected in the function q.

Minimizing the Kullback–Leibler divergence is the same as maximizing the log-likelihood function, which is the essence of the Maximum Likelihood Estimation method:

$$\hat{t}_{\text{MLE}} = \underset{t \in [0,N)}{\operatorname{argmax}} \mathcal{L}(t|q)$$

Setting the derivative of the log-likelihood function to zero gives the equation for Maximum Likelihood Estimate:

$$\begin{aligned} 0 &= \frac{\partial}{\partial t} \log \mathcal{L}(t|q)(\hat{t}_{\mathrm{MLE}}) \\ 0 &= \frac{\partial}{\partial t} \sum_{k=0}^{N-1} q(k) \log(p_{N,t}(k))(\hat{t}_{\mathrm{MLE}}) \\ \cot(\hat{t}_{\mathrm{MLE}}\pi) &= \frac{1}{N} \sum_{k=0}^{N-1} q(k) \cot((\hat{t}_{\mathrm{MLE}} - k)\frac{\pi}{N}) \end{aligned} \tag{5}$$

Note that if $q = p_{N,t}$ (an ideal measurement) then $\hat{t}$ satisfies the equation as reflected in the identity in the preliminaries (Eq. 5).

This method has the benefit of well-understood theory, including confidence intervals. However, the likelihood function built from measurements on quantum devices in the NISQ era may diverge significantly from the true one. Figure 2 plots the likelihood function for various t values using experiments run on real quantum devices. These experiments are discussed in detail in Section 6.

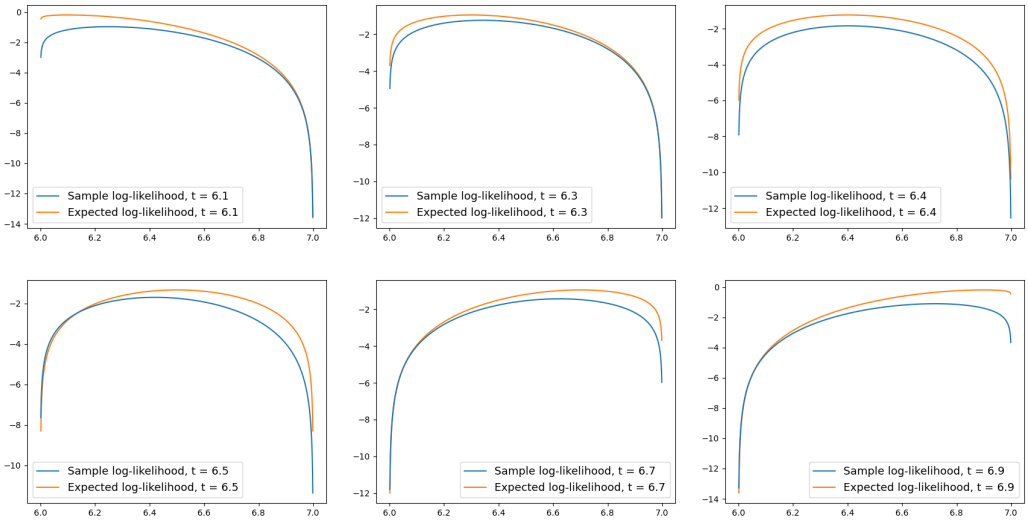


Figure 2: The theoretical log-likelihood function compared to the log-likelihood using measurement probabilities from experiments on *ibm_perth* $\log \mathcal{L}(t|q)$ for several values t.

3 Discrete Sinc Quantum State and Fejér Distribution Properties

In this section we provide properties of the discrete sinc quantum state that are essential to the design of estimators in the next section.

Lemma 3.1. *For a non-integer value $t \in (0, N)$ and an integer $0 \leq k < N-1$ we have*

$$c_{N,t}(k) = (-1)^{\lfloor t \rfloor - k} \operatorname{sgn}(\lfloor t \rfloor - k) \sqrt{p_{N,t}(k)}$$

where $\operatorname{sgn}(x) = -1$ if $x < 0$ and $\operatorname{sgn}(x) = 1$ if $x \geq 0$.

Proof.

$$\begin{aligned} c_{N,t}(k) &= \frac{1}{N} \frac{\sin((t-k)\pi)}{\sin((t-k)\frac{\pi}{N})} \\ &= \frac{1}{N} \frac{(-1)^{\lfloor t \rfloor - k} |\sin(t\pi)|}{\operatorname{sgn}(\lfloor t \rfloor - k) |\sin((t-k)\frac{\pi}{N})|} \\ &= (-1)^{\lfloor t \rfloor - k} \operatorname{sgn}(\lfloor t \rfloor - k) \sqrt{p_{N,t}(k)} \end{aligned}$$

□

Lemma 3.2 (Ratio-Based Estimation)**.** *Given a non-integer value $t \in (0, N)$ we have*

$$\tan((t-k)\frac{\pi}{N}) = \frac{\sin\frac{\pi}{N}}{\cos\frac{\pi}{N} + \sqrt{\frac{p_{N,t}(k)}{p_{N,t}(k+1)}}}, \tag{6}$$

for an integer $0 \leq k < N-1$, and

$$\tan((t-N+1)\frac{\pi}{N}) = \frac{\sin\frac{\pi}{N}}{\cos\frac{\pi}{N} - \sqrt{\frac{p_{N,t}(N-1)}{p_{N,t}(0)}}}. \tag{7}$$

Proof. The following proves Eq. 6:

$$\begin{aligned}
\sqrt{\frac{p_{N,t}(k)}{p_{N,t}(k+1)}} &= \frac{c_{N,t}(k)}{c_{N,t}(k+1)} \\
&= -\frac{\sin((t-k-1)\frac{\pi}{N})}{\sin((t-k)\frac{\pi}{N})} \\
&= -\frac{\sin((t-k)\frac{\pi}{N})\cos\frac{\pi}{N} - \cos((t-k)\frac{\pi}{N})\sin\frac{\pi}{N}}{\sin((t-k)\frac{\pi}{N})} \\
&= -\cos\frac{\pi}{N} + \frac{1}{\tan((t-k)\frac{\pi}{N})}\sin\frac{\pi}{N}
\end{aligned}$$

Therefore,

$$\tan((t-k)\frac{\pi}{N}) = \frac{\sin\frac{\pi}{N}}{\cos\frac{\pi}{N} + \sqrt{\frac{p_{N,t}(k)}{p_{N,t}(k+1)}}}.$$

□

Corollary 3.2.1. *For $t \in (k, k+1)$ and an integer $0 \leq k < N-1$ we have*

$$t = k + \frac{N}{\pi}\arctan\left(\frac{\sin\frac{\pi}{N}}{\cos\frac{\pi}{N} + \sqrt{\frac{p_{N,t}(k)}{p_{N,t}(k+1)}}}\right).$$

If $t \in (N-1, N)$ an adjustment needs to be made to the formula:

$$t = N - 1 + \frac{N}{\pi}\arctan\left(\frac{\sin\frac{\pi}{N}}{\cos\frac{\pi}{N} - \sqrt{\frac{p_{N,t}(N-1)}{p_{N,t}(0)}}}\right).$$

These are also an analytical solutions for Eq. 5.

Lemma 3.3 (Coin Approximation)**.** *Given a non-integer value $t \in (k, k+1)$ and an integer $0 \leq k < N-1$, if N is sufficiently large the decimal part of t can be approximated by*

$$\begin{aligned}
t - k &\approx \frac{1}{1 + \sqrt{\frac{p_{N,t}(k)}{p_{N,t}(k+1)}}} \\
&= \frac{\sqrt{p_{N,t}(k+1)}}{\sqrt{p_{N,t}(k)} + \sqrt{p_{N,t}(k+1)}}.
\end{aligned}$$

Proof. Given the fact that when N is sufficiently large, $\frac{1}{N}$ is close to 0, we can approximate $\sin\left(\frac{\pi}{N}\right)$ by $\frac{\pi}{N}$, $\tan\left((t-k)\frac{\pi}{N}\right)$ by $(t-k)\frac{\pi}{N}$, and $\cos\left(\frac{\pi}{N}\right)$ by 1 in Eq. 6 and Eq. 7. □

Corollary 3.3.1. *The decimal part of t can be approximated as the bias of a coin that lands heads-up $\lfloor M\sqrt{p_{N,t}(k+1)}\rfloor$ times and tails-up $\lfloor M\sqrt{p_{N,t}(k)}\rfloor$ times, where the integer factor M is chosen based on the desired precision.*

Lemma 3.4 (Interpolation Formula)**.** *Combining the classical interpolation theorem [1] and Lemma 3.1, for a well-behaved (periodic, band limited as in [2]) function $f : \{0,\ldots,N-1\} \to \mathbb{R}$:*

$$f(t) = \sum_{k=0}^{N-1} f\left(\frac{k}{N}\right) c_{N,t}(k) = \sum_{k=0}^{N-1} f\left(\frac{k}{N}\right) (-1)^{\lfloor t\rfloor - k} \operatorname{sgn}(\lfloor t\rfloor - k)\sqrt{p_{N,t}(k)}$$

4 Applications to Quantum Measurement Interpolation

Assume we have an n-qubit quantum register whose state is the result of encoding a value, following the quantum phase estimation procedure. The value could represent the phase of a unitary operator's eigenvalue, as in the original context of quantum phase estimation, the probability of marked states, as in the quantum amplitude estimation context, encoding function values, etc.

With the notation $N = 2^n$, we interpret the encoded value as a real number $t \in [0, N)$. In some contexts we may be interested in the value $\frac{t}{N} \in [0, 1)$. The state of the register will reflect the quantum state in Eq. 1.

Repeated measurements of the state of the register create a sample from the probability distribution $p_{N,t}$ as in Eq. 3. We denote by q the function that maps the outcome k, for $0 \le k < N$, corresponding to the computational state $|k\rangle_n$ to the proportion (normalized count) of measurements of the outcome k.

Ratio-Based Estimation As discussed in Lemma 3.2, using the formulas in Corollary 3.2.1, the ratio of amplitudes can be used to get an estimate for the value t:

$$\hat{t}_{\mathrm{RBE}} = \lfloor t\rfloor + \frac{N}{\pi}\arctan\left(\frac{\sin\frac{\pi}{N}}{\cos\frac{\pi}{N} + \sqrt{q(\lfloor t\rfloor)/q(\lceil t\rceil)}}\right) \tag{8}$$

or

$$\hat{t}_{\mathrm{RBE}} = \lceil t\rceil - \frac{N}{\pi}\arctan\left(\frac{\sin\frac{\pi}{N}}{\cos\frac{\pi}{N} + \sqrt{q(\lceil t\rceil)/q(\lfloor t\rfloor)}}\right), \tag{9}$$

where we can infer the ceiling and floor of t from the measurements (top two largest values of q). We abbreviate this method by "RBE".

Coin Approximation Estimation As discussed in Lemma 3.3, the magnitudes of the amplitudes of the floor and ceiling of the value t (i .e. the amplitudes with the largest magnitudes) can be used as likelihoods for the sides of a coin whose bias is an estimate for $t - \lfloor t\rfloor$, the decimal part of t.

We can use one of many available methods to estimate the bias of this Bernoulli process. This approach has the benefit of well-understood theory and known confidence/credible intervals.

In our experiments we have used the Bayesian approach that relies on the fact that the Beta distribution is the conjugate prior of the Bernoulli distribution. The posterior distribution is the Beta distribution with the square roots of the two largest sampling counts as parameters.

Interpolation-Based Estimation Using the interpolation formula in Lemma 3.4 with a well-behaved function (e.g $x \mapsto \cos(x\pi)$) we get

$$\cos(\hat{t}\pi) \approx \sum_{k=0}^{N-1} \cos\left(\frac{k}{N}\pi\right)(-1)^{\lfloor t \rfloor - k}\,\mathrm{sgn}(\lfloor t \rfloor - k)\sqrt{q(k)}.$$

Then we can solve for $\hat{t}$.

5 Confidence Intervals for Ratio-Based and Coin Approximation Estimators

For an integer $n > 1$ and a real number $t \in (k, k+1)$, where $N = 2^n$ and $0 \leq k < N$, consider the state $|\phi_{n,t}\rangle$ defined in Eq. 1. For a positive integer L, and a sequence of L measurements of this state, denote by r the ratio of the normalized measurement frequencies of the states $|k\rangle$ and $|k+1\rangle$, and by s the sum of these frequencies. Then, according to Eq. 8, the decimal part of t depends only on N and r, and not on k, and is defined by:

$$D_N(r) = \frac{N}{\pi}\arctan\left(\frac{\sin\frac{\pi}{N}}{\cos\frac{\pi}{N} + \sqrt{r}}\right). \tag{10}$$

Since the ratio estimator is asymptotically normally distributed [8], we can use the delta method [9] to derive a $100(1-\alpha)\%$ confidence interval for the estimator of the decimal part of t:

$$\left[D_N(r) - z_{\alpha/2}\frac{\sigma D'_N(r)}{L}, D_N(r) + z_{\alpha/2}\frac{\sigma D'_N(r)}{L}\right]$$

where $\sigma = (1+r)\sqrt{\frac{r}{s}}$, and $z_{\alpha/2}$ denotes the normal critical value corresponding to the significance level $\alpha \in (0,1)$.

Credible intervals for the Coin Approximation Estimator can be computed using the percent point function of the Beta distribution. Figure 3 compares the radius of the intervals using these two methods.

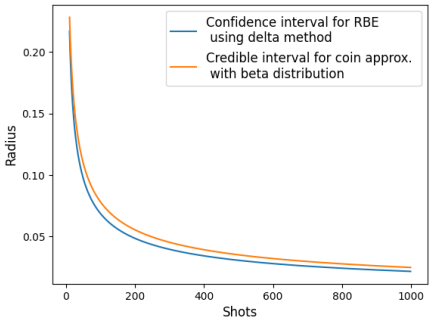


Figure 3: The radius of the RBE confidence interval compared to the Coin Approx. credible interval using the theoretical measurement frequencies of the highest two measurements given $n = 3, N = 8$ and $t = 4.2$, for a given number of shots.

6 Numerical Experiments

In this section we perform experiments for an empirical analysis of the methods described in the previous section on both quantum simulators and quantum computers. We use IBM Quantum services to perform the experiments [10]. Details about the systems and configurations can be found in Appendix C.

Using the value encoding algorithm described in [2] to prepare the state $|\phi_{n,t}\rangle$ as defined in Eq. 1 using n-qubits and a given value $t \in [0, 2^n)$. Each circuit is run with $20,000$ shots. The

memory parameter in IBM Quantum services [11] allows for the measurement at each shot to be retrieved. We refer to the measuremnt at a given shot as a sample.

Given a round of samples, we estimate the parameter t using the MLE method discussed in Lemma 2.1 (Eq . 5), as well as the Ratio-Based Estimation (RBE) and Coin Approximation estimation methods introduced Section 4. Interpolation-Based Estimation is not included because it did not perform well in experiments.

6.1 Quantum Simulator Experiments

The estimations from experiments performed on a quantum simulator backend were both highly accurate and highly precise. Figure 4 visualizes 20 estimations for values of t at increments of 0.1 in between 6.1 and 6.9 using three different estimation methods: RBE, Coin Approximation and MLE. The average error of the 20 estimates is low for all three methods, and it is difficult to determine if any method gives better estimates.

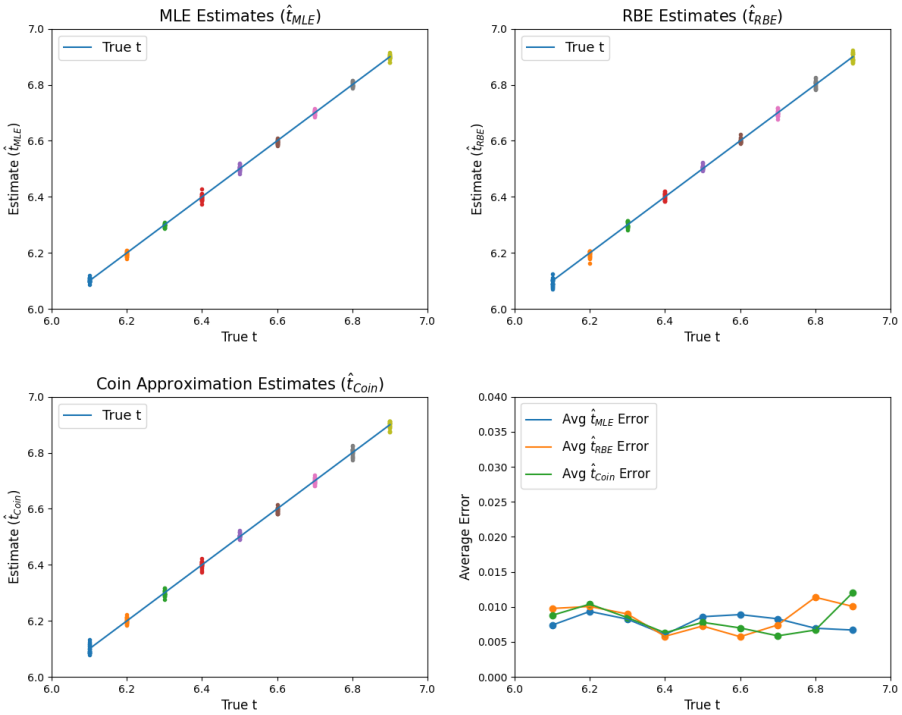


Figure 4: Top Left: MLE estimates for t computed using 1,000 samples from quantum simulator experiments with $n = 3$ qubits and values of t at increments of 0.1 in between 6.1 and 6.9. Top Right: RBE estimates for t computed using 1,000 samples from quantum simulator experiments with $n = 3$ qubits and values of t at increments of 0.1 in between 6.1 and 6.9. Bottom Left: Coin Approximation estimates for t computed using 1,000 samples from quantum simulator experiments with $n = 3$ qubits and values of t at increments of 0.1 in between 6.1 and 6.9. Bottom Right: The average error of estimates computed using samples from experiments on a quantum simulator.

6.2 Quantum Hardware Experiments

Figures 5 and 6 visualize the measurement frequencies from experiments using 3 qubits on *ibm_perth* and estimates for various values of t. Each estimate is computed using a set of $1,000$ samples, and we repeat the process for 20 rounds. Figure 5 compares estimates computed using MLE and RBE methods and Figure 6 compares estimates computed using MLE and Coin Approximation Estimation.

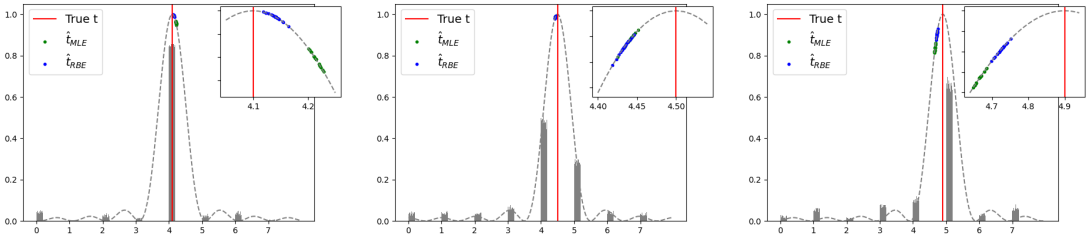


Figure 5: The histograms of normalized measurement probabilities for each set of 1,000 samples from experiments with $n = 3$ qubits and $t = 4.1$, $t = 4.5$ and $t = 4.9$ on *ibm_perth*, compared to the expected probability distribution defined in Eq. 3. For each set of 1,000 samples, we compute estimates using MLE and RBE.

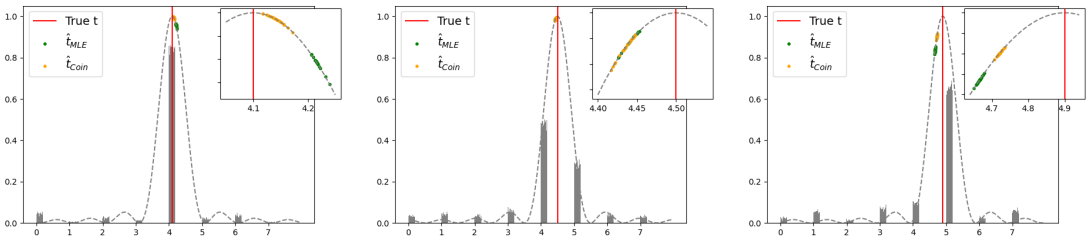


Figure 6: The histograms of normalized measurement probabilities for each set of 1,000 samples from experiments with $n = 3$ qubits and $t = 4.1$, $t = 4.5$ and $t = 4.9$ on *ibm_perth*, compared to the expected probability distribution defined in Eq. 3. For each set of 1,000 samples, we compute estimates using MLE and Coin Approximation Estimation.

As mentioned in Section 2, results from experiments on real quantum hardware in the NISQ era show much more divergence from the true likelihood function than results from quantum simulation. Figure 7 visualizes results from 20 rounds with $1,000$ samples each for values of t at increments of 0.1 in between 6.1 and 6.9 using a 3 qubits on *ibm_perth*.

The experiment was repeated for various intervals of t using 3 and 4 qubit registers on *ibm_perth*. Results from these additional experiments are included in Appendix D.

7 Concluding Remarks

In this paper we explore a few methods for estimating the decimal part of a number encoded through the Phase or Amplitude Estimation Algorithm.

The full interpolation method and the Maximum Likelihood Estimation method use sampling counts for all possible outcomes, and give good theoretical results, but it turns out that they are sensitive to noise when implemented on quantum hardware that is currently available, without additional error correction. Methods that rely on only the top two counts seem to be less sensitive to such noise, and they are also simple to use, providing closed forms for the decimal of the encoded value for the given counts. Confidence/credible intervals for these methods are also relatively simple to obtain.

Acknowledgements

The views expressed in this article are those of the authors and do not represent the views of Wells Fargo. This article is for informational purposes only. Nothing contained in this article should be construed as investment advice. Wells Fargo makes no express or implied warranties and expressly disclaims all legal, tax, and accounting implications related to this article.

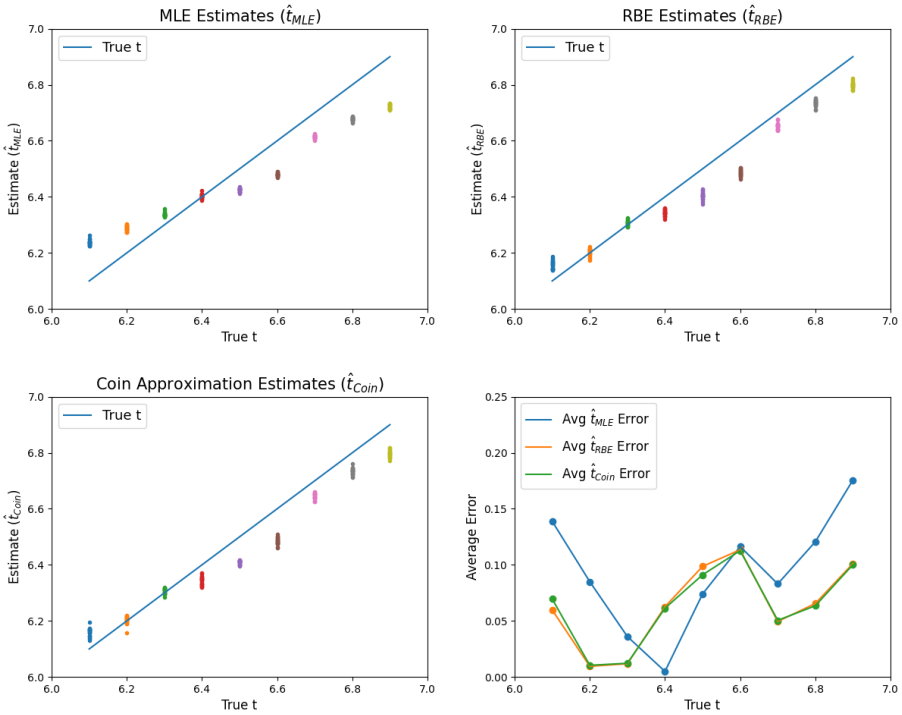


Figure 7: Top Left: MLE estimates for t computed using 1,000 samples from experiments on *ibm_perth* with $n = 3$ qubits and values of t at increments of 0.1 in between 6.1 and 6.9. Top Right: RBE estimates for t computed using 1,000 samples from experiments on *ibm_perth* with $n = 3$ qubits and values of t at increments of 0.1 in between 6.1 and 6.9.. Bottom Left: Coin Approximation estimates for t computed using 1,000 samples from experiments on *ibm_perth* with $n = 3$ qubits and values of t at increments of 0.1 in between 6.1 and 6.9. Bottom Right: The average error of estimates computed using samples from experiments on a quantum simulator.

We acknowledge the use of IBM Quantum services for this work. The views expressed are those of the authors, and do not reflect the official policy or position of IBM or the IBM Quantum team.

References

[1] Chapter 3 from the course mat-inf2360. URL https://www.uio.no/studier/emner/matnat/math/nedlagte-emner/MAT-INF2360/.

[2] Charlee Stefanski, Vanio Markov, and Constantin Gonciulea. Quantum amplitude interpolation, 2022. URL https://arxiv.org/abs/2203.08758.

[3] Kenneth Hoffman. *Banach spaces of analytic functions*. Dover, Mineola, NY, 2007.

[4] Svante Janson. Moments of gamma type and the brownian supremum process area. *Probab. Surveys*, 7:1–52, 2010. DOI: 10.1214/10-PS160. URL https://doi.org/10.1214/10-PS160.

[5] Dmitry Grinko, Julien Gacon, Christa Zoufal, and Stefan Woerner. Iterative quantum amplitude estimation. *npj Quantum Information*, 7(1), mar 2021. DOI: 10.1038/s41534-021-00379-1. URL https://doi.org/10.1038%2Fs41534-021-00379-1.

[6] Ronald N. (Ronald Newbold) Bracewell. *The Fourier transform and its applications*, chapter The Filtering or Interpolating Function, sincx. McGraw-Hill series in electrical and computer engineering. Circuits and systems. McGraw Hill, Boston, 3rd ed. edition, 2000. ISBN 0073039381.

[7] Vanio Markov, Charlee Stefanski, Abhijit Rao, and Constantin Gonciulea. A generalized quantum inner product and applications to financial engineering, 2022. URL https://arxiv.org/abs/2201.09845.

[8] Frantisek Duris, Juraj Gazdarica, Iveta Gazdaricova, Lucia Striskova, Jaroslav Budis, Jan Turna, and Tomas Szemes. Mean and variance of ratios of proportions from categories of a

multinomial distribution. *Journal of Statistical Distributions and Applications*, 5, 2, January 201. DOI: https://doi.org/10.1186/s40488-018-0083-x.
[9] Goerge Casella and Roger Berger. *Statistical Inference*. Thomson Learning, 2002.
[10] IBM Quantum, 2021. URL https://quantum-computing.ibm.com/.
[11] Qiskit: An open-source framework for quantum computing, 2021.

A Addtional Properties of the Discrete Sinc Quantum State

The following additional identities can be useful in further understanding the discrete sinc quantum state and associated Fejér distribution.

Lemma A.1. *Given a non-integer $t \in (0, N)$ and an integer $0 \leq k < N$ we have*

$$\tan((t-k)\frac{\pi}{N}) = \sqrt{\frac{p_{N,t}\left((k+\frac{N}{2}) \mod N\right)}{p_{N,t}(k)}}$$

$$\sum_{k=0}^{N-1} \sin((t-k)\frac{\pi}{N})c_{N,t}(k) = 0$$

$$\sum_{k=0}^{N-1} \cos((t-k)\frac{\pi}{N})c_{N,t}(k) = 1$$

$$\sum_{k=0}^{N-1} (-1)^k \sin((t-k)\frac{\pi}{N})c_{N,t}(k) = \sin(t\pi)$$

$$\sum_{k=0}^{N-1} e^{i\pi\frac{N-1}{N}k} c_{N,t}(k) = e^{i\pi\frac{N-1}{N}t}$$

$$\sum_{k=0}^{N-1} (-1)^k \cos(k\frac{\pi}{N})c_{N,t}(k) = \cos(t\frac{N-1}{N}\pi)$$

$$\sum_{k=0}^{N-1} (-1)^k \sin(k\frac{\pi}{N})c_{N,t}(k) = -\sin(t\frac{N-1}{N}\pi)$$

$$\frac{1}{N}\sum_{k=0}^{N-1} \cot((t-k)\frac{\pi}{N}) = \cot(t\pi)$$

B Estimator Analysis

For a positive integer L, and a sequence of L measurements of the state $|\phi_{n,t}\rangle$ defined in Eq . 1 (where n is a positive integer, $N = 2^n$ and $t \in [0, N)$), we denote by r the ratio of the probabilities of the states $|k\rangle$ and$|k+1\rangle$. We denote by $\hat{r}$ the estimator of this ratio. Following [8], we analyze the expectation and variance of $\hat{r}$.

The expectation of $\hat{r}$ is

$$\mu_{\hat{r}} = \frac{p_{N,t}(k)}{p_{N,t}(k+1)}\left(1 + \frac{1}{Lp_{N,t}(k+1)}\right), \tag{11}$$

and its variance is

$$\sigma^2_{\hat{r}} = \frac{1}{L}\left(\frac{p_{N,t}(k)}{p_{N,t}(k+1)}\right)^2\left(\frac{1}{p_{N,t}(k)} + \frac{1}{p_{N,t}(k+1)}\right) \tag{12}$$

where $p_{N,t}$ is defined in Eq. 3 and $0 \leq k < N$.

Figure 8 shows samples of the expectation and variance compared to the theoretical values.

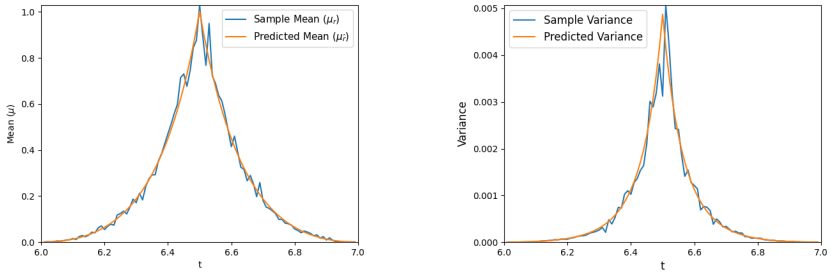


Figure 8: Left: The expectation of $\hat{r}$ defined in Eq. 11 compared to measured values of r from a quantum simulator for $L = 1,000$ samples, $n = 3$ qubits and values of $t \in (6, 7)$. Right: The predicted variance of $\hat{r}$ defined in Eq. 12 compared to the variance of measured values of r from 100 rounds using a quantum simulator for $L = 1,000$ samples, $n = 3$ qubits and values of $t \in (6, 7)$. In both figures, we use the opposite ratio for values of t with a decimal part greater than 0.5 to keep the ratio less than 1.

Using the Taylor expansion of the function D_N defined in Eq. 10, we can compute the expectation and variance of the estimator.

The expectation is

$$E(\hat{t}_{\mathrm{RBE}}) \approx D'_N(\mu_{\hat{r}}) + \frac{D''_N(\mu_{\hat{r}})}{2}\sigma^2_{\hat{r}}, \tag{13}$$

and the variance is

$$\mathrm{Var}(\hat{t}_{\mathrm{RBE}}) \approx D'_N(\mu_{\hat{r}})^2\sigma^2_{\hat{r}} - \frac{1}{4}D''_N(\mu_{\hat{r}})^2\sigma^2_{\hat{r}} \tag{14}$$

where $\hat{t}_{\mathrm{RBE}}$ is defined in Eq. 8.

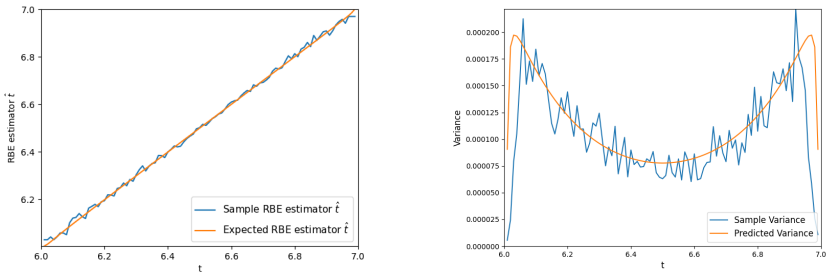


Figure 9: Left: The expectation of $\hat{t}_{\mathrm{RBE}}$ defined in Eq. 13, with $\mu_{\hat{r}}$ defined in Eq. 11, $\sigma^2_{\hat{r}}$ defined in Eq . 12 and $L = 1000$, compared to $\hat{t}_{\mathrm{RBE}}$ computed using 1,000 samples from a quantum simulator with $n = 3$, and values of $t \in (6, 7)$. Right: The variance of $\hat{t}_{\mathrm{RBE}}$ defined in Eq. 14, with $\mu_{\hat{r}}$ defined in Eq. 11, $\sigma^2_{\hat{r}}$ defined in Eq. 12 and $L = 1000$, compared to the variance of 100 $\hat{t}_{\mathrm{RBE}}$ values computed using 1,000 samples from a quantum simulator.

C Hardware Details

These experiments were run on the IBM Quantum system *ibm_perth*, which a IBM Quantum Falcon processor with 7 qubits. The error map at the time of the experiments is shown in Figure 10. Each circuit in the experiment was measured with 20,000 shots. Relevant calibration data is included in Figure 10 and Table 1.

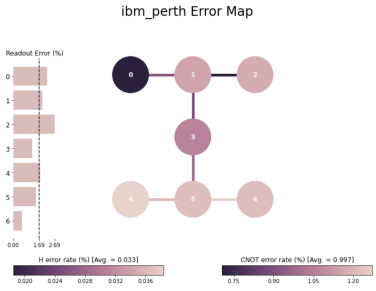


Figure 10: Error map of *ibm_perth* generated at the time of the experiments. The three qubit circuits were run on qubits $1, 3, 5$. The four qubit circuits were run on $3, 4, 5, 6$. The six qubit circuits were run on $0, 1, 3, 4, 5, 6$.

Qubit pair	Error (%)	Qubit	T_1 (μs)	T_2 (μs)
(0, 1)	0.918	Q0	147	85
(1, 3)	0.890	Q1	218	57
(3, 5)	0.990	Q3	130	127
(4, 5)	1.203	Q4	155	165
(5, 6)	1.271	Q6	199	155
Average	1.05±0.17			

Table 1: Calibration data from *ibm_perth* from calibration before experiments.

D Additional Quantum Hardware Experiments

Figures 11 and 12 visualize the results of experiments run on *ibm_perth* with 3 and 4 qubits, respectively, for more intervals of t.

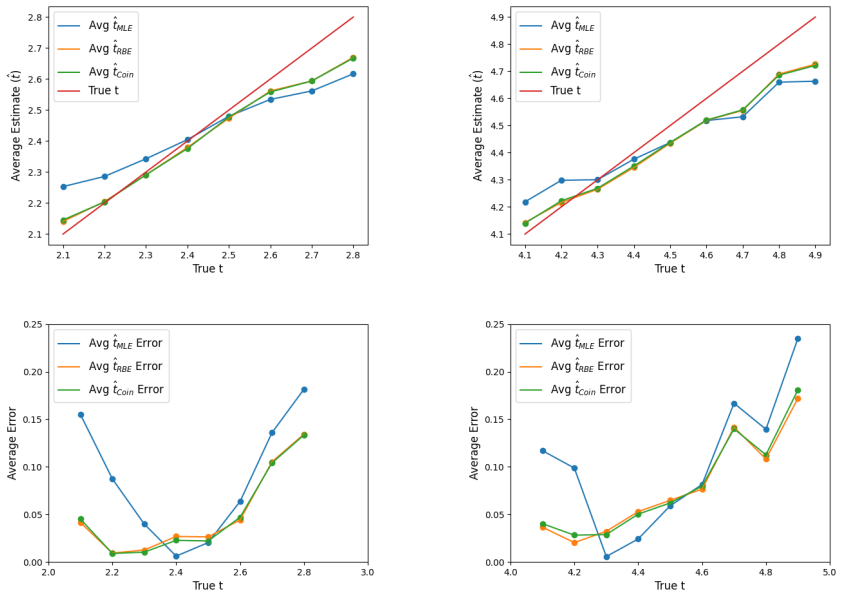


Figure 11: Left: The average of 20 estimates using each of the three methods (MLE, RBE, and Coin Approximation) from experiments on *ibm_perth* with $n = 3$ qubits and values of t at increments of 0 .1 in between 2.1 and 2.9 and the average error of the respective estimates. Right: The average of 20 estimates using each of the three methods (MLE, RBE, and Coin Approximation) from experiments on *ibm_perth* with $n = 3$ qubits and values of t at increments of 0.1 in between 4.1 and 4.9, and the average error of the respective estimates.

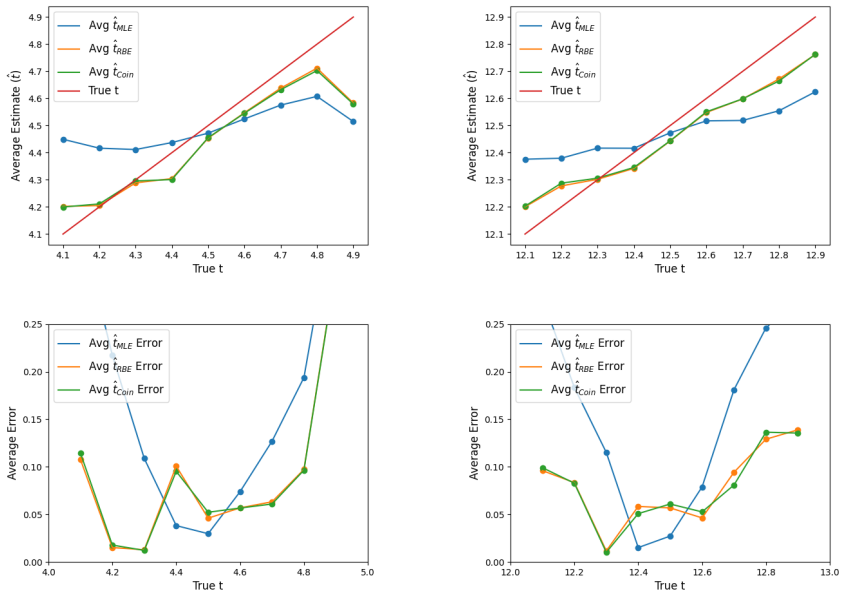


Figure 12: Left: The average of 20 estimates using each of the three methods (MLE, RBE, and Coin Approximation) from experiments on *ibm_perth* with $n = 4$ qubits and values of t at increments of 0 .1 in between 4.1 and 4.9, and the average error of the respective estimates. Left: The average of 20 estimates using each of the three methods (MLE, RBE, and Coin Approximation) from experiments on *ibm_perth* with $n = 4$ qubits and values of t at increments of 0.1 in between 12.1 and 12.9, and the average error of the respective estimates.